

Lifelong reinforcement learning for health-aware fast charging of lithium-ion batteries

Meng Yuan^a, Changfu Zou^{a,*}

^a*Department of Electrical Engineering, Chalmers University of Technology, Gothenburg, 41296, Sweden*

Abstract

Fast charging of lithium-ion batteries remains a critical bottleneck for widespread adoption of electric vehicles and stationary energy storage systems, as improperly designed fast charging can accelerate battery degradation and shorten lifespan. In this work, we address this challenge by proposing a health-aware fast charging strategy that explicitly balances charging speed and battery longevity across the entire service life. The key innovation lies in establishing a mapping between anode overpotential and the state of health (SoH) of battery, which is then used to constrain the terminal charging voltage in a twin delayed deep deterministic policy gradient (TD3) framework. By incorporating this SoH-dependent voltage constraint, our designed deep learning method mitigates side reactions and effectively extends battery life. To validate the proposed approach, a high-fidelity single particle model with electrolyte is implemented in the widely adopted PyBaMM simulation platform, capturing degradation phenomena at realistic scales. Comparative life-cycle simulations against conventional CC-CV, its variants, and constant current–constant overpotential methods show that the TD3-based controller reduces overall degradation while maintaining competitively fast charge times. These results demonstrate the practical viability of deep reinforcement learning for advanced battery management systems and pave the way for future explorations of health-aware, performance-optimized charging strategies.

Keywords: Lithium-ion battery, fast charging, reinforcement learning, battery degradation.

1. Introduction

Lithium-ion batteries (LIBs) have emerged as the cornerstone of modern energy storage systems, powering applications ranging from portable electronics to electric vehicles (EVs) and grid-scale renewable energy integration [1, 2]. Despite their dominance, EVs continue to face two persistent challenges, limited driving range and prolonged charging durations, which remain critical barriers to their widespread adoption and the push for energy-efficient electrification [3, 4]. The energy density, charge and discharge kinetics of LIBs are primarily determined by their electrochemical composition, including cathode and anode materials and electrolytes, as well as their structural design, such as particle morphology and electrode architecture [5]. While advancements in battery chemistry continue to push theoretical limits of battery, sophisticated battery management systems (BMS) have shown promise in optimizing charging

*Corresponding author.

Email addresses: meng.yuan@chalmers.se (Meng Yuan), changfu.zou@chalmers.se (Changfu Zou)

protocols to achieve fast charging without exceeding intrinsic material constraints [6]. Though effective in reducing charging time, unconstrained high-current charging accelerates capacity fade through mechanisms such as lithium plating and solid-electrolyte interphase (SEI) growth [7]. To address this dilemma, advanced control algorithms capable of dynamically balancing charging speed and longevity, through multi-physics-aware current modulation and degradation-predictive interventions, are urgently required to unlock the full potential of LIBs [8].

Accurate battery modeling is essential for designing health-aware fast charging control algorithms. One widely used approach is the equivalent circuit model (ECM), which simulates voltage dynamics using simplified resistor-capacitor networks and offers computational efficiency ideal for real-time embedded systems [9, 10, 11]. However, without modeling the first principles underlying intercalation reactions and the diffusion process within battery cells, ECMs often struggle to capture locally distributed behavior, particularly those related to safety and aging. In contrast, electrochemical models, such as the Doyle-Fuller-Newman (DFN) model, explicitly describe ion transport and reaction kinetics across electrode microstructures, enabling physics-based predictions of degradation modes [12, 13]. Yet, the significant computational burden of solving the coupled partial differential equations (PDEs) inherent in the DFN models limits their practical application in advanced control methods that also demand high computational power. To address these challenges, the single particle model (SPM) has emerged as a pragmatic simplification. By assuming a uniform electrolyte concentration, the SPM reduces PDEs to a set of ordinary differential equations (ODEs) while still capturing essential electrochemical behavior [14]. Recent work has extended the SPM to incorporate various capacity fade mechanisms and integrated it into a model predictive control (MPC) framework to optimize charging profiles and minimize intra-cycle capacity fade [15]. However, the conventional SPM neglects electrolyte dynamics and leads to significant voltage prediction errors at high C-rates, which has motivated the development of extensions such as the single particle model with electrolyte (SPMe) for improved accuracy [16, 17, 18].

Conventional lithium-ion battery charging typically employs the constant current–constant voltage (CC-CV) method, where the battery is first charged at a fixed current until a set voltage is reached, and then held at constant voltage while the current gradually decreases. Although fast charging can be achieved by increasing the current or target voltage, such measures tend to accelerate battery degradation phenomena such as lithium plating, thereby reducing battery life [19]. To solve this issue, researchers turned to health-aware fast charging strategies that integrate battery degradation models with advanced control techniques. In [20], an anode overpotential based PID controller is designed to mitigate the risks of lithium plating while increasing the speed of charging. In [21], Yang et al. proposed a constant-overpotential based fast charging strategy for Li-ion batteries and show that this constant-overpotential control outperforms the traditional CC-CV protocol in both charging speed and lithium-plating suppression. Similarly, Lu et al. developed a model predictive control (MPC) framework that incorporates real-time lithium plating detection and adaptive parameter updates to optimize the balance between fast charging and long-term battery health [22]. However, this model based approach is not adaptive to the parameters variation during battery degradation. Moreover, the overpotential is hard to be measured in practical application, which hinders the implementation of overpotential based method. This challenge has inspired the development of various approaches, such as machine learning-based

methods, to estimate lithium plating [23].

To address the challenges of model mismatch and parameter drift as batteries age, learning-based methods have been introduced in the field of battery charging. In [24], a deep reinforcement learning (RL) based approach has been designed for the fast charging of battery, and two cases considering if the overpotential is measurable are discussed in the design of the controller. While the method shows promise for rapid charging, it models battery aging solely as an increase in film resistance, and the controller design does not integrate long-term battery degradation considerations. In [25], Wei et al. propose a deep RL-based strategy for the fast charging of lithium-ion batteries, specifically targeting thermal safety and health-conscious charging. The multiphysics-related constraints are implicitly incorporated into the reward design of the RL. However, the agent is trained on a per-episode basis, with the battery model initialized at the beginning of each epoch. In [26], an adaptive model-based RL strategy leverages Gaussian processes to capture the battery environment and enforce operational constraints during charging, but its primary focus is on minimizing charging time rather than extending battery life.

Based on the discussion above, our work addresses the challenge in fast charging by taking battery degradation into explicit account throughout the entire lifespan. We employ a twin delayed deep deterministic policy gradient (TD3) method for health-aware fast charging. To mitigate battery degradation, we first establish a mapping between the side-reaction overpotential and the charge cut-off voltage and then integrate it as health-related constraint into the training of our RL agent. The SPMe coupling degradation is employed as the battery environment to capture electrochemical behavior. The contributions of this work are summarized as follows:

1. Unlike previous approaches that focus solely on minimizing charging time while only implicitly incorporating constraints to extend battery life, this introduces the first explicit formulation of lifelong battery fast charging problem, aiming at reducing charging duration while extending longevity of battery.
2. A mapping between the charge cut-off voltage and SoH is established using a constant current (CC)–constant overpotential (COP) approach. This mapping leverages the intrinsic relationship between the anode overpotential and battery degradation, and can be integrated into both CCCV-based charging and learning-based advanced charging, allowing directly incorporation of battery health into charging control.
3. By integrating the obtained mapping between the voltage and SoH, a TD3-based charging strategy is designed to explicitly optimize the fast charging process.
4. The proposed TD3-based strategy is trained and tested through comprehensive life-cycle simulations using the battery simulator Python Battery Mathematical Modeling (PyBaMM) [27] with a SPMe-aging model. Superior performance is demonstrated over CC-CV charging and its variants.

The rest of this paper is organized as follows. The SPMe model with integrated degradation mechanisms is described in Section 2. The health-aware fast charging problem and the proposed TD3 based charging approach are formulated in Section 3, followed by the effectiveness analysis and comparative studies in Section 4. Section 5 concludes this work.

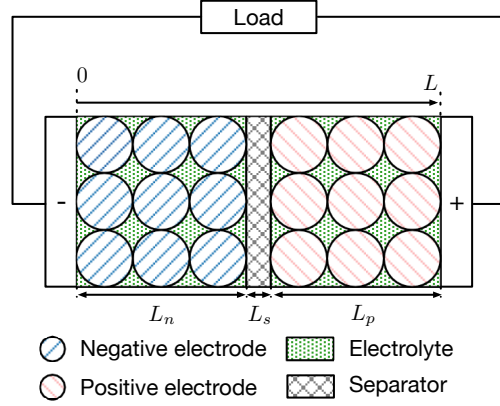


Figure 1: The internal structure of a lithium-ion battery cell (modified from [17]).

2. Electrochemical model with degradation mechanism

The DFN model, also known as the pseudo-two-dimensional (P2D) model, is a widely used electrochemical framework for simulating lithium-ion battery behavior [28]. In addition to the required heavy computation, the DFN model relies on a large number of parameters, many of which are difficult to measure accurately, leading to challenges in calibration [29]. To overcome these issues, the SPMe model reduces the computational burden and the number of parameters needed [16], making it a suitable model when designing the charging strategy of battery with consideration of whole life performance.

2.1. Single particle model with electrolyte

The structure of a lithium-ion battery is illustrated in Figure 1, where the negative electrode, separator, and positive electrode have thicknesses L_n , L_s , and L_p , respectively. The SPMe model approximates each electrode as a single spherical particle, assuming that the solid-phase concentration is uniformly distributed along the thickness direction, denoted by x . Under this assumption, the diffusion process inside the spherical particle is governed by

$$\frac{\partial c_{s,i}}{\partial t}(r, t) = \frac{D_{s,i}}{r^2} \frac{\partial}{\partial r} \left(r^2 \frac{\partial c_{s,i}}{\partial r}(r, t) \right), \quad i \in \{n, p\}, \quad (1)$$

where r represents the distance from the center of the spherical particle, t is time, $c_{s,i}$ is the solid-phase lithium-ion concentration, and $D_{s,i}$ is its diffusivity.

The electrolyte diffusion equations for the negative electrode, separator, and positive electrode are given by:

$$\frac{\partial c_{e,n}}{\partial t}(x, t) = \frac{\partial}{\partial x} \left(\frac{D_{e,n}^{\text{eff}}(c_{e,n})}{\varepsilon_{e,n}} \frac{\partial c_{e,n}}{\partial x}(x, t) \right) + \frac{1 - t_c}{\varepsilon_{e,n} F L_n} I(t), \quad (2)$$

$$\frac{\partial c_{e,\text{sep}}}{\partial t}(x, t) = \frac{\partial}{\partial x} \left(\frac{D_{e,\text{sep}}^{\text{eff}}(c_{e,\text{sep}})}{\varepsilon_{e,\text{sep}}} \frac{\partial c_{e,\text{sep}}}{\partial x}(x, t) \right), \quad (3)$$

$$\frac{\partial c_{e,p}}{\partial t}(x, t) = \frac{\partial}{\partial x} \left(\frac{D_{e,p}^{\text{eff}}(c_{e,p})}{\varepsilon_{e,p}} \frac{\partial c_{e,p}}{\partial x}(x, t) \right) + \frac{1 - t_c}{\varepsilon_{e,p} F (L - L_p)} I(t), \quad (4)$$

where $c_{e,i}$ is the lithium-ion concentration in the electrolyte, $D_{e,i}^{\text{eff}}(c_{e,i})$ is the effective diffusion coefficient, $\varepsilon_{e,i}$ is the volume fraction of electrolyte in the region $i \in \{n, \text{sep}, p\}$, t_c is the transference number, F is the Faraday constant, and I is the applied current to the system.

The electric potential in each electrode i is given by

$$\phi_{s,i}(x, t) = \eta_i(t) + \phi_{e,i}(x, t) + U_i(c_{ss,i}(t)) + FR_{f,i}j_{n,i}(t), \quad i \in \{n, p\}, \quad (5)$$

where c_{ss} is the solid-phase lithium-ion concentration on the particle surface. The overpotential $\eta_i(t)$ is computed by solving the Butler-Volmer equation regarding $j_{n,i}$ and is given as:

$$\eta_i(t) = \frac{RT}{\alpha F} \sinh^{-1} \left(\frac{\mp I(t)}{2a_i L_i I_{0,i}(t)} \right), \quad i \in \{n, p\}, \quad (6)$$

where α is the charging transfer coefficient, R is the universal gas constant, T is the absolute temperature, a_i is the surface area per unit volume of the electrode particles. The electrolyte potential is computed as:

$$\phi_e(L, t) - \phi_e(0, t) = \frac{L_n + 2L_s + L_p}{2\kappa} I(t) + \frac{2RT}{F} (1 - t_c) k_f(t) (\ln c_e(L, t) - \ln c_e(0, t)), \quad (7)$$

where κ is the electrolyte conductivity which is approximately constant in c_e , $k_f(t) \triangleq (1 + (d \ln f_{c/a} / d \ln c_e))$ and $f_{c/a}$ is the activity coefficient ratio.

The boundary conditions for the solid-phase diffusion (1) are:

$$\frac{\partial c_{s,i}}{\partial r}(0, t) = 0, \quad i \in \{n, p\} \quad (8)$$

$$\frac{\partial c_{s,n}}{\partial r}(R_{s,n}, t) = -\frac{1}{D_{s,n} F a_n L_n} I(t), \quad (9)$$

$$\frac{\partial c_{s,p}}{\partial r}(R_{s,p}, t) = \frac{1}{D_{s,p} F a_p (L - L_p)} I(t). \quad (10)$$

The corresponding boundary conditions for electrolyte diffusion equations (2) - (4) are:

$$\frac{\partial c_{e,n}}{\partial x}(0, t) = \frac{\partial c_{e,p}}{\partial x}(L, t) = 0, \quad (11)$$

$$D_{e,n}^{\text{eff}}(L_n) \frac{\partial c_{e,n}}{\partial x}(L_n, t) = D_{e,\text{sep}}^{\text{eff}}(L_n) \frac{\partial c_{e,\text{sep}}}{\partial x}(L_n, t), \quad (12)$$

$$D_{e,\text{sep}}^{\text{eff}}(L - L_p) \frac{\partial c_{e,\text{sep}}}{\partial x}(L - L_p, t) = D_{e,p}^{\text{eff}}(L - L_p) \frac{\partial c_{e,p}}{\partial x}(L - L_p, t), \quad (13)$$

$$c_{e,n}(L_n, t) = c_{e,\text{sep}}(L_n, t), \quad (14)$$

$$c_{e,\text{sep}}(L - L_p, t) = c_{e,p}(L - L_p, t). \quad (15)$$

The nonlinear output of terminal voltage $V(t)$ is computed as:

$$V(t) = \phi_{s,p}(L, t) - \phi_{s,n}(0, t). \quad (16)$$

2.2. Battery degradation mechanisms

Battery performance and lifetime are limited by several degradation mechanisms [30]. In this study, we focus on two dominant degradation processes, namely the SEI layer growth and lithium plating. The idea is that suppressing them during fast charging may significantly extend battery lifetime.

2.2.1. SEI growth model

The SEI layer forms on the anode particle surface and significantly affects the lifetime of lithium-based batteries. SEI growth is primarily a diffusion-limited process, in which solvent molecules react with lithiated graphite. To accurately capture this process, we utilize a two-layer diffusion-limited SEI growth model described in [31]. In this model, the inner and outer SEI layers are assumed to grow simultaneously at the same rate. Consequently, two differential equations, one describing each layer, are integrated into the SPMe to track their evolution over time:

$$\frac{\partial L_{\text{inner}}}{\partial t} = \frac{c_{\text{sol},0} D_{\text{sol}}(T) \bar{V}_{\text{SEI}}}{4L_{\text{inner}}}, \quad (17)$$

$$\frac{\partial L_{\text{outer}}}{\partial t} = \frac{c_{\text{sol},0} D_{\text{sol}}(T) \bar{V}_{\text{SEI}}}{4L_{\text{outer}}}, \quad (18)$$

where $c_{\text{sol},0}$ is the bulk solvent concentration and \bar{V}_{SEI} is SEI partial molar volume; $D_{\text{sol}}(T)$ is the temperature-dependent diffusion coefficient described by Arrhenius relation. The SEI layer causes a voltage drop as:

$$\eta_{\text{SEI}} = \rho_{\text{SEI}}(L_{\text{inner}} + L_{\text{outer}}) \frac{j_{\text{tot}}}{a_-}, \quad (19)$$

where ρ_{SEI} is the SEI Ohmic resistivity, and j_{tot} is interfacial current density.

2.2.2. Lithium plating model

To capture how active lithium ions decay into dead lithium over time, the following equation is introduced [31]:

$$\frac{\partial c_{\text{Li}}}{\partial t} = -a_- N_{\text{Li}} - \gamma(L_{\text{SEI}}) c_{\text{Li}}. \quad (20)$$

where the decay rate γ is a SEI thickness dependent parameter. The concentration of the dead lithium c_{dLi} is given by:

$$\frac{\partial c_{\text{dLi}}}{\partial t} = \gamma(L_{\text{SEI}}) c_{\text{Li}}, \quad (21)$$

The Li stripping flux N_{Li} is updated using Butler-Volmer equation as [32, 33]:

$$N_{\text{Li}} = k_{\text{Li}} \left(c_{\text{Li}} \exp\left(\frac{F\alpha_{a,\text{Li}}\eta_{\text{stripping}}}{RT}\right) - c_e \exp\left(\frac{-F\alpha_{c,\text{Li}}\eta_{\text{stripping}}}{RT}\right) \right), \quad (22)$$

where

$$\eta_{\text{stripping}} = \phi_s - \phi_e - \eta_{\text{SEI}}. \quad (23)$$

Recent studies have indicated that degradation mechanisms, particularly lithium plating, are strongly influenced by the anode overpotential and can significantly limit battery performance and lifespan [34, 35]. This anode overpotential is described as:

$$\eta_{\text{side}}(x, t) = \phi_{s,n} - \phi_{e,n} - U_{\text{side}}, \quad (24)$$

where U_{side} is the equilibrium potential of the side reaction, assumed to be zero for lithium plating [32].

The initial partial differential algebraic equation (DAE) model can be reformulated and reduced as a DAE model by suitable numerical methods, such as finite difference and spectral methods [36, 37]:

$$\dot{x} = f(x, z, u), \quad (25)$$

$$y = h(x, z, u), \quad (26)$$

$$0 = g(x, z, u), \quad (27)$$

where $x = [c_{s,n}, c_{s,p}, c_e]^\top \in \mathbb{R}^{n_x}$ is the state vector, $z = [\phi_{s,n}, \phi_{s,p}, \phi_e, i_{e,n}, i_{e,p}]^\top \in \mathbb{R}^{n_z}$ is the algebraic variable vector, $y = [V, \text{SoC}, \text{SoH}]^\top$ is the output and $u \triangleq I$ is the applied input current.

3. Health-aware fast charging problem

A battery is considered to have reached its end of life when its SoH falls to a specified threshold, such as 75-80% for EV applications. Within this health-aware fast charging framework, we aim to minimize the charging time needed to reach the desired SoC while maximizing the number of equivalent full cycles (EFCs) of battery until the SOH reaches 80%. The cost function for this problem is defined as:

$$J(t) = w_1 C_{\text{SoC}}(t) + w_2 C_{\text{side}}(t), \quad (28)$$

where w_1 and w_2 are weighting factors. The first part of the cost is designed for SoC setpoint tracking, aiming to minimize charging duration. The cost function is defined as:

$$C_{\text{SoC}}(t) = |\text{SoC}^* - \text{SoC}(t)|, \quad (29)$$

where SoC^* denotes the target state of charge, and SoC_t represents the current state of charge. Considering the lithium plating is the main degradation mechanism here, the degradation-related cost is defined as:

$$C_{\text{side}}(t) = |\eta_{\text{side}}(t) - \eta_{\text{min}}|, \quad (30)$$

where η_{min} is a predefined threshold overpotential, below which battery degradation becomes excessively rapid. We can interpret this threshold as follows: when the anode overpotential falls below this value, further reducing it to achieve faster charging is no longer beneficial, as the resulting acceleration in battery degradation outweighs any additional gains in charging speed.

The constraint of this problem involves that the input current is limited by the battery charger as:

$$0 \leq I(t) \leq I_{\text{max}}. \quad (31)$$

Then, the health-aware fast charging problem is formulated as

$$\begin{aligned}
& \min_{I(t)} \int_0^{t_e} J(t) dt \\
& \text{s.t. Battery dynamics: } (2)-(7), (17)-(24), \\
& \quad \text{Input constraints: } (31), \\
& \quad \text{SoC}(t_f) = \text{SoC}^*, \quad \forall \text{ cycles}, \\
& \quad \text{SoH}(t_e) = \text{SoH}_{\text{end}}, \tag{32}
\end{aligned}$$

where t_f denotes the charging completion time for each cycle, which can vary over the lifespan of battery, t_e represents the end-of-life time of the battery, and SoH_{end} is the specified battery SoH at end-of-life, set to 80% in this study.

This optimization problem is formulated to minimize the overall cost function over the battery lifetime from initial time 0 to its end-of-life time t_e . Each charging cycle within this period terminates at time t_f when the SoC reaches the target SoC^* .

3.1. Constant current constant overpotential based control

To solve the fast charging problem as shown in (32), one intuitive idea is to design the controller based on overpotential feedback. This constant current-constant overpotential (CC-COP) method mirrors the traditional CC-CV approach by initiating with a constant current phase, followed by dynamically regulating the anode potential to a small positive value using real-time feedback. This method has been shown to effectively reduce the risk of plating by maintaining the electrode overpotential at a safe, constant level after the initial current phase [21, 23].

However, the CC-COP control in fast charging faces two significant limitations: Firstly, measuring electrode potentials directly in commercial batteries is challenging as it requires advanced sensors typically used only in laboratory settings, making it impractical for widespread application. Secondly, determining the appropriate overpotential threshold is not straightforward. While setting a high threshold can help reduce lithium plating, it may result in overly conservative charging corresponding to very long charging times. The need to finely tune the overpotential threshold adds complexity to real-world implementation, further complicating the adoption of CC-COP control strategies in commercial battery charging systems. These issues are further illustrated through high-fidelity simulations in a later section.

3.2. Reinforcement learning based fast charging algorithm

In this subsection, we introduce a twin delayed deep deterministic policy gradient (DDPG) based method to solve the health-aware fast charging problem defined in (32). Figure 2 illustrates the overall system structure, which includes three main components. The first component is a battery environment that integrates a lithium-ion battery model accounting for battery degradation, as discussed in Section 2. Within this environment, we establish a correlation between the target voltage and the SoH using CC-COP control. This correlation provides important battery health

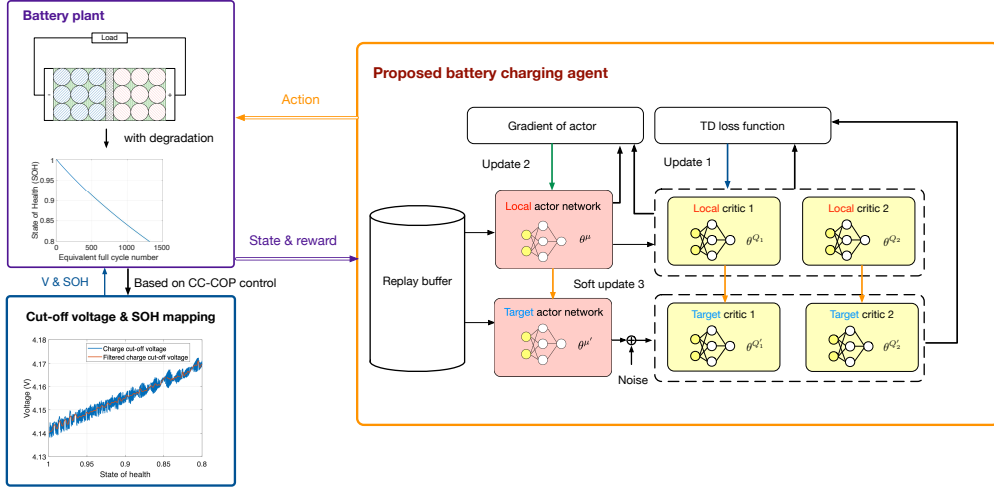


Figure 2: Structure of the proposed method.

information to the environment, enabling the generation of reward signals for the battery charging agent. The third and key component of this work is the TD3-based battery charging agent, which utilizes state information and reward signals from the battery environment to determine optimal charging actions. The specifics of this method are detailed further below.

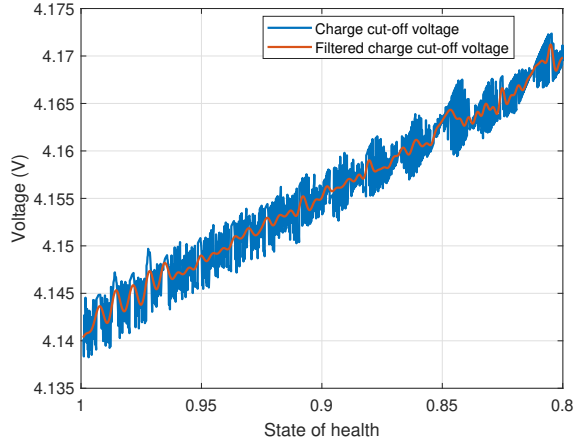


Figure 3: Mapping between SoH and charge cut-off voltage at 80% SoC based on CC-COP control.

Since the anode overpotential is challenging to be measured in practical applications, the CC-COP method can instead be implemented in a laboratory environment. Our objective here is to design a controller based on the insights provided by the CC-COP controller. We employ the designed CC-COP controller as detailed in Section 3.1 and identify the maximum terminal voltage of the battery cell, $V_{\text{cut-off}}$, during each charging process that consistently aims for the SoC setpoint, SoC^* . This voltage identification continues until the SoH of battery falls below 80%, signaling the end of its lifespan. The obtained relationship between $V_{\text{cut-off}}$ and SoH is illustrated in Figure 3. Although the CC-COP

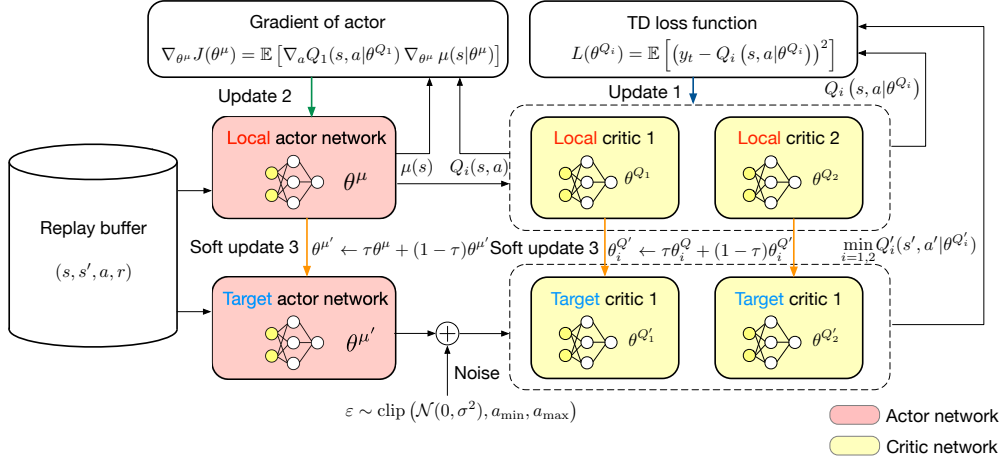


Figure 4: Structure of the deep learning algorithm.

method depends on feedback from overpotential, this mapping offers valuable insights for developing a methodology that considers battery health without directly relying on overpotential measurements. As the SoH decreases from 1.0 to 0.8, the target voltage gradually increases from approximately 4.14 V to roughly 4.17 V. This indicates that a more degraded battery requires a higher terminal voltage to achieve the same charge level when using overpotential-based feedback.

3.2.1. TD3 method overview

To address the charging problem specified in (32), the TD3 algorithm, an enhanced version of the DDPG framework, aims to rectify the Q-value overestimation issue inherent in DDPG. It introduces targeted improvements that boost the learning stability and accuracy. The architecture of the TD3 algorithm is illustrated in Figure 4. Within the Actor-Critic framework, TD3 incorporates two types of networks: the critic network $Q(s, a|\theta^Q)$ with parameter θ^Q and the actor network $\mu(s|\theta^\mu)$ with parameter θ^μ . To mitigate the overestimation of the Q-value, TD3 employs a technique that calculates the target Q-value by selecting the lesser value from the two target critic networks, effectively reducing potential overestimation:

$$y_t(r, s') = r(s, a) + \gamma \min_{i=1,2} Q'_i(s', a'|\theta^{Q_i}), \quad (33)$$

where y_t is the target Q-value for given state s and action a ; a' is the next action chosen by the policy based on next state s' ; γ is the discounting factor; θ^{Q_i} is the parameter of target critic. The critic network updates its parameters based on gradient descent applied to the loss function as follows:

$$L(\theta^{Q_i}) = \mathbb{E} \left[\left(y_t - Q_i(s, a|\theta^{Q_i}) \right)^2 \right], \quad (34)$$

$$\nabla_{\theta^{Q_i}} L(\theta^{Q_i}) = \mathbb{E} \left[\left(y_t - Q_i(s, a|\theta^{Q_i}) \right) \nabla_{\theta^{Q_i}} Q_i(s, a|\theta^{Q_i}) \right], \quad (35)$$

where $\mathbb{E}(\cdot)$ denotes the expectation operator, θ^{Q_i} is the parameter of Q_i . As indicated in Figure 4, the parameter is updated (Update 1) according to:

$$\theta^{Q_i} \leftarrow \theta^{Q_i} - \alpha \nabla_{\theta^{Q_i}} L(\theta^{Q_i}), \quad (36)$$

where α is the learning rate of the critic network. Moreover, TD3 reduces instability by postponing updates to its actor network relative to its critic. In practice, the critic is updated frequently to accurately capture the dynamics of environment, while the actor is adjusted only after a fixed number of critic updates. This delay minimizes error propagation and keeps the policy changes smoother, resulting in more stable and reliable learning outcomes. The actor network is updated (Update 2) with parameters using gradient ascent of the objective function as:

$$J_Q(\theta^\mu) = \mathbb{E}[Q_1(s, \mu(s))], \quad (37)$$

$$\nabla_{\theta^\mu} J_Q(\theta^\mu) = \mathbb{E}\left[\nabla_a Q_1(s, a|\theta^{Q_1}) \nabla_{\theta^\mu} \mu(s|\theta^\mu)\right], \quad (38)$$

$$\theta^\mu \leftarrow \theta^\mu + \beta \nabla_{\theta^\mu} J_Q(\theta^\mu), \quad (39)$$

where θ^μ is the parameter of actor network, $J(\theta^\mu)$ is the defined objective function, $\nabla_{\theta^\mu} J(\theta^\mu)$ is the gradient of objective function with respect to θ^μ , β is the learning rate of the policy network. As denoted as Soft update 3 in the Figure 4, the parameters of the target critic and the target actor network are updated as:

$$\theta_i^{Q'} \leftarrow \tau \theta_i^Q + (1 - \tau) \theta_i^{Q'}, \quad (40)$$

$$\theta^{\mu'} \leftarrow \tau \theta^\mu + (1 - \tau) \theta^{\mu'}, \quad (41)$$

where the soft updating factor is denoted by τ and $\theta^{\mu'}$ is the parameter of the target actor network.

Furthermore, TD3 introduces truncated normal noise to the actions produced by the target policy network, mitigating the trade-off between bias and variance. This added noise serves as a form of regularization, which helps prevent overestimation of Q-values and reduces the risk of overfitting. By smoothing the target updates in this manner, TD3 achieves more stable learning and enhances the reliability of policy evaluation:

$$a_{t+1} \leftarrow \mu'(s'|\theta^{\mu'}) + \varepsilon, \quad \varepsilon \sim \text{clip}\left(\mathcal{N}(0, \sigma^2), a_{\min}, a_{\max}\right), \quad (42)$$

where a_{\min} and a_{\max} define the valid range of actions, representing the lower and upper bounds of the battery charging current, respectively.

3.2.2. Battery application

For the TD3-based fast charging algorithm, the battery SoC and voltage are chosen as the state variables:

$$s(t) = [V(t), \text{SoC}(t)]^\top. \quad (43)$$

The action of the agent is the charge current value:

$$a(t) = I(t), \quad s.t. (31). \quad (44)$$

With the established voltage-to-SoH mapping and the TD3 algorithm described above, we define the reward function to address the optimization problem in (32), achieving fast charging while minimizing battery degradation:

$$r(t) = r_{\text{SoC}}(t) + r_{\text{vol}}(t) + r_{\text{smooth}}(t). \quad (45)$$

To encourage fast charging, the SoC-related reward is defined as:

$$r_{\text{SoC}}(t) = \lambda_{\text{SoC}} |\text{SoC}^* - \text{SoC}(t)|, \quad (46)$$

where λ_{SoC} is a weighting factor that quantifies the importance of rapidly reaching the target SoC. To mitigate risks associated with lithium plating, the terminal voltage is constrained by the SoH-dependent upper bound, $V_{\text{max}}(\text{SoH})$:

$$r_{\text{vol}}(t) = \begin{cases} \lambda_{\text{vol}} |V(t) - V_{\text{max}}(\text{SoH})|, & V(t) > V_{\text{max}}(\text{SoH}), \\ 0, & \text{otherwise,} \end{cases} \quad (47)$$

where λ_{vol} is a weighting factor representing the importance of adhering to the voltage limit.

Additionally, to encourage gradual variations in the charging current and prevent abrupt control actions that may stress the battery, we introduce a smoothness term:

$$r_{\text{smooth}}(t) = \lambda_{\text{smooth}} |a(t) - a(t-1)|, \quad (48)$$

where λ_{smooth} is a tuning parameter that penalizes rapid changes in the control input.

It is important to note that, despite the value of SoH being used to update the voltage constraints, it does not appear as a direct term in the reward function. Instead, the influence of SoH is embedded within the dynamic adjustment of V_{max} and the value of V_{max} ensuring that the reinforcement learning policy naturally adapts to the aging mechanism of battery without penalizing the agent explicitly for changes in SoH.

4. Health-aware fast charging results

In this section, we aim to evaluate the proposed RL-based charging strategy using high-fidelity simulations and compare it against widely adopted charging control strategies, such as CC-CV and CC-COP control. We enhance the CC-CV method by adjusting the constant voltage stage based on the V_{cutoff} -SoH mapping, as described in Section 3.2. This modified approach is termed as the CC-CV with varying voltage (CC-CV-V) method, which aims to account for the SoH during battery charging. Additionally, we explore the constant current-constant overpotential method as a benchmark controller, setting the overpotential reference to two distinct values: $\eta_{\text{side}}^* = 0.01$ V for a conservative charging strategy, and $\eta_{\text{side}}^* = -0.05$ V for an aggressive approach. These variants are named CC-COP-slow and CC-COP-fast, respectively, and are used for comparative analysis.

The open-source PyBaMM software (version 24.5), is employed as the simulation platform [27], in which the SPMe-aging model from Section 2 is implemented. As detailed in Section 2, the battery model features a single particle model with an electrolyte component, which facilitates efficient and comprehensive analysis of cycle aging. The

investigated battery is an LG M50 cell, with electrochemical parameters obtained from [31]. The main degradation mechanisms include SEI growth, governed by a solvent diffusivity of 2.5×10^{-22} m²/s.

The main degradation mechanisms are characterized by an SEI solvent diffusivity of 2.5×10^{-22} m²/s, a lithium plating kinetic rate constant of 1×10^{-11} m/s, and an irreversible condition for lithium plating.

In this study, we implement a unified procedure to assess the performance of various charging strategies over the entire life of the battery. The details of this process are shown as Protocol 1. This protocol includes an initial stage to obtain the actual capacity of battery, followed by repeated testing cycles using different charging controls. The primary objective of this comprehensive battery life testing is to evaluate the effectiveness of these controls in optimizing the charging process and extending the operational lifespan of the battery.

Protocol 1 Battery cycling protocol for controller investigation

- 1: **Initialize:** Discharge the battery to 0% SoC.
 - 2: **Charge** to 100% SoC using CC-CV.
 - 3: **Discharge** the battery completely to determine actual capacity.
 - 4: **repeat**
 - 5: **Charge** the battery from 0% SoC to 20% SoC using low-current CC strategy.
 - 6: **Rest** for one hour.
 - 7: **Apply** the target charging strategy to charge the battery to 80% SoC.
 - 8: **Discharge** the battery to 0% SoC.
 - 9: **Rest** for one hour.
 - 10: **Check** SoH; if SoH falls to SoH_{end} (e.g., 80%), end test.
 - 11: **until** battery SoH \leq SoH_{end}
 - 12: **Evaluate** performance based on total cycles in terms of the averaged charging time and the equivalent full cycles.
-

4.1. Training of the proposed method

The proposed controller employs an actor-critic neural network architecture. The actor and critic networks each contain two fully connected hidden layers with 200 units per layer. The hyperparameters of training are summarized in Table 1. The penalty coefficients in the proposed controller are chosen as $\lambda_{\text{SoC}} = -2$, $\lambda_{\text{vol}} = -10$, and $\lambda_{\text{smooth}} = -0.5$, respectively. The maximum control input is limited as $I_{\text{max}} = 10\text{A}$.

The training performance of the proposed charging algorithm is presented in Figure 5, illustrating the evolution of four critical metrics across approximately 2000 episodes. The evaluations were conducted at 20 episode intervals. Figure 5a shows the cumulative reward, which initially fluctuates significantly around -2000 due to the exploration of highly conservative charging strategies but stabilizes near -60 after approximately 1000 episodes, indicating convergence to a policy effectively reducing charging time while extending battery life. The large initial negative values

Table 1: Hyperparameter of the proposed TD3 algorithm

Hyperparameters	Values
Actor network learning rate	0.0001
Critic network learning rate	0.0001
Discounting factor	0.99
Experience replay buffer size	1.0×10^6
Minibatch size	256
Soft update factor	0.005
Delay frequency	1

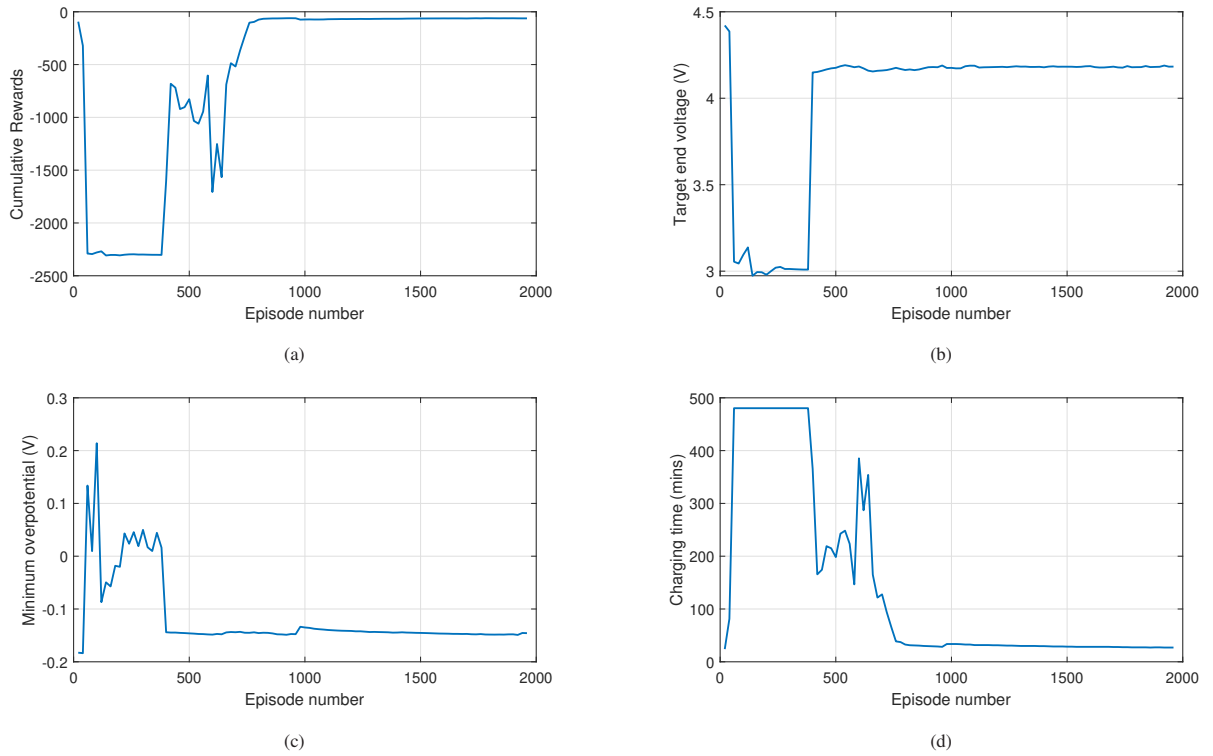


Figure 5: The training performance of the proposed method: (a) cumulative rewards; (b) maximum end voltage; (c) minimum overpotential η_{side} ; (d) charging time.

result from assigning a substantial negative reward (-1000) whenever the charging time exceeds 480 minutes. Figure 5b depicts the charge cut-off voltage, which initially oscillates around 3.5 V but stabilizes around 4.2 V after 1000 episodes, demonstrating the ability of algorithm to maintain an optimal voltage threshold guided by the V_{cutoff} -SoH mapping. Additionally, Figure 5c illustrates the convergence behavior of the minimum overpotential, showing that its value stabilizes around -0.145 V. Figure 5d demonstrates that, in general, higher cumulative rewards during training

correlate with reduced charging times. The charging time ultimately stabilizes near 27 minutes in later episodes.

4.2. Fast charging results

Table 2: Battery charging performance based on different methods

	Maximum EFCs	Average charging time (mins)
CC-CV	572	24.15
CC-CV-V	611	24.14
CC-COP-slow*	1316	36.02
CC-COP-fast*	1009	22.40
Proposed method	703	24.12

* Requires side-reaction overpotential measurements.

Following the battery cycling protocol as described in Protocol 1, we conducted the battery charging tests using five different strategies: the CC-CV strategy, the CC-CV-V strategy, two CC-COP strategies, and the proposed approach. A finer sampling resolution can better capture the transient dynamics of batteries, but at the expense of computational efficiency. In this study, the primary metrics of interest are battery lifetime and charging time. Considering these factors, the sampling time for the lifelong implementation of all these strategies was set as 20 s. The EFCs and the average charging time for these approaches are summarized in Table 2.

4.2.1. Overall analysis on charging time and lifespan

Among the methods, the CC-COP controllers rely fully on the measurement of side-reaction overpotential, and demonstrate performance variation depending on the tuning of the desired overpotential reference. The CC-COP-fast strategy achieves the shortest average charging time of 22.40 minutes and significantly extends the battery lifetime compared to CC-CV methods, with 1009 EFCs. In comparison, the CC-COP-slow strategy attains the longest battery lifespan, which is 1316 FECS, yet requires the longest charging time of 36.02 minutes, reflecting a very conservative strategy.

Different from CC-COP strategies, the proposed approach along with CC-CV and CC-CV-V exhibit more practical applicability and deployability. The variation in battery SOH with respect to EFCs for these three methods is presented in Figure 6. The baseline CC-CV method, despite achieving a competitive charging time of 24.15 minutes, suffers from the shortest battery lifespan with 572 EFCs. This limitation stems from its rigid voltage and current thresholds during the charging process, which fail to adapt to battery degradation dynamics. The CC-CV-V strategy addresses this weakness by incorporating V_{cutoff} -SOH mapping to dynamically adjust the charge cut-off voltage. This modification yields a modest lifespan improvement with 611 EFCs while maintaining near-identical charging speed with 24.14 minutes. However, the 6.8% improvement of EFCs over CC-CV suggests that static parameter mapping alone cannot fully capture complex aging mechanisms.

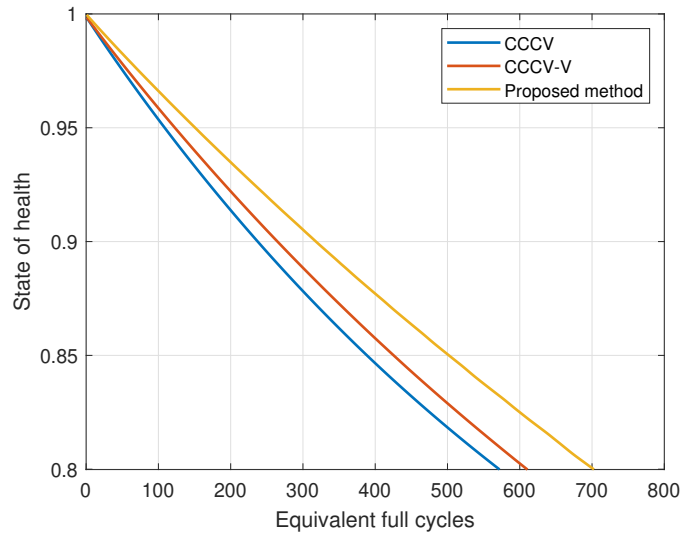


Figure 6: Comparison of SoH degradation among different charging methods.

In contrast, the proposed method achieves a significant improvement in performance, where battery lifespan is extended to 703 EFCs (23% and 15% higher than CC-CV and CC-CV-V, respectively) while marginally reducing charging time to 24.12 minutes. This breakthrough results from its health-aware control architecture, which integrates indirect degradation indicators to dynamically optimize charging protocols.

In summary, compared to CC-COP strategies, the proposed method achieves enhanced practicality for real-world deployment by eliminating the need for specialized overpotential sensors, despite its slightly longer charging time and fewer equivalent full cycles than CC-COP-fast and CC-COP-slow approaches. In contrast to CC-CV and its variants, the proposed approach maintains comparable charging efficiency while largely extending battery lifespan, demonstrating that lifespan enhancement can be achieved without compromising charging speed.

4.2.2. Charging time dynamics over battery aging

Figure 7 compares five charging strategies in terms of charging time versus SoH. Overall, the CC-COP-slow method exhibits the longest charging durations across the SoH range, starting at approximately 40 minutes when the battery is fully healthy and dropping to around 30 minutes when SoH reaches 80%. The charging times of all methods decrease as SoH declines, primarily because less energy or charge capacity is absorbed by the battery for the same SoC change. The CC-CV, CC-CV-V, and proposed methods exhibit generally similar trajectories, though CC-CV-V notably shows a substantial peak at the beginning and subsequently decreases more rapidly than the CC-CV and the proposed method. By contrast, the proposed method maintains a relatively stable decrease in charging time compared to the other methods.

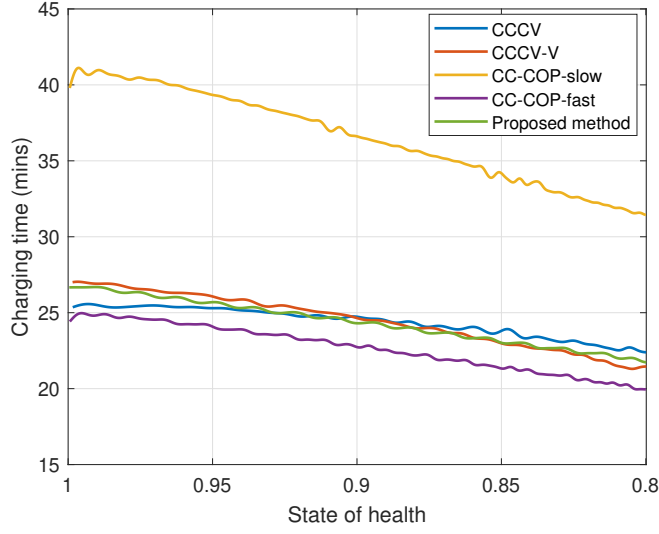


Figure 7: Charging time based on different charging approaches.

4.2.3. Evolution of current and overpotential profiles

To further investigate why the proposed learning-based method effectively extends the battery lifespan compared to CC-CV and its variants, the battery current and anode overpotential profiles during a single charging process are plotted for two distinct aging stages. Specifically, results from the 1st cycle (new battery) and the 200th cycle (aged battery) are presented in Figure 8.

Figure 8 illustrates distinct shifts in anode overpotential profiles across different charging methods when comparing new and aged cells. For aged cells, a clear downward and leftward shift in the overpotential curves is observed, indicating that the same charging current results in lower overpotential as the cell ages. This phenomenon is particularly pronounced in the CC-CV and CC-CV-V charging methods. In contrast, the current profiles of the proposed method behave like a multi-stage constant-current scheme that results in smoother current and anode potential transitions in both new and aged cells. The TD3-based method significantly reduces the difference in anode potentials between new and aged cells, indicating its ability to attenuate the effects of battery aging.

Regarding overpotential levels, the proposed approach only remains at a relatively low negative value for a short period before moving the anode potential closer to zero. By contrast, the overpotential under CCCV and its variants methods remains below -0.05 V for most of the charge and lasts for nearly 15 minutes. This prolonged negative overpotential may thermodynamically favor lithium plating, thereby increasing the risk of degradation and reducing long-term battery health compared to the proposed method.

These results not only facilitate a comparison between the different controllers but also highlight the discrepancies in performance of the same controller at different stages of battery aging. Such insights are especially meaningful for researchers and engineers seeking to optimize fast charging strategies.

4.2.4. Capacity loss due to lithium plating

Finally, we analyze the relative difference in capacity loss for CC-CV and CC-CV-V, compared to the proposed method, as a function of SoH, as shown in Figure 9. This difference is expressed as a percentage of the baseline capacity loss for each strategy. Positive values indicate that the proposed method yields a lower capacity loss than conventional strategies, highlighting its effectiveness in extending battery life.

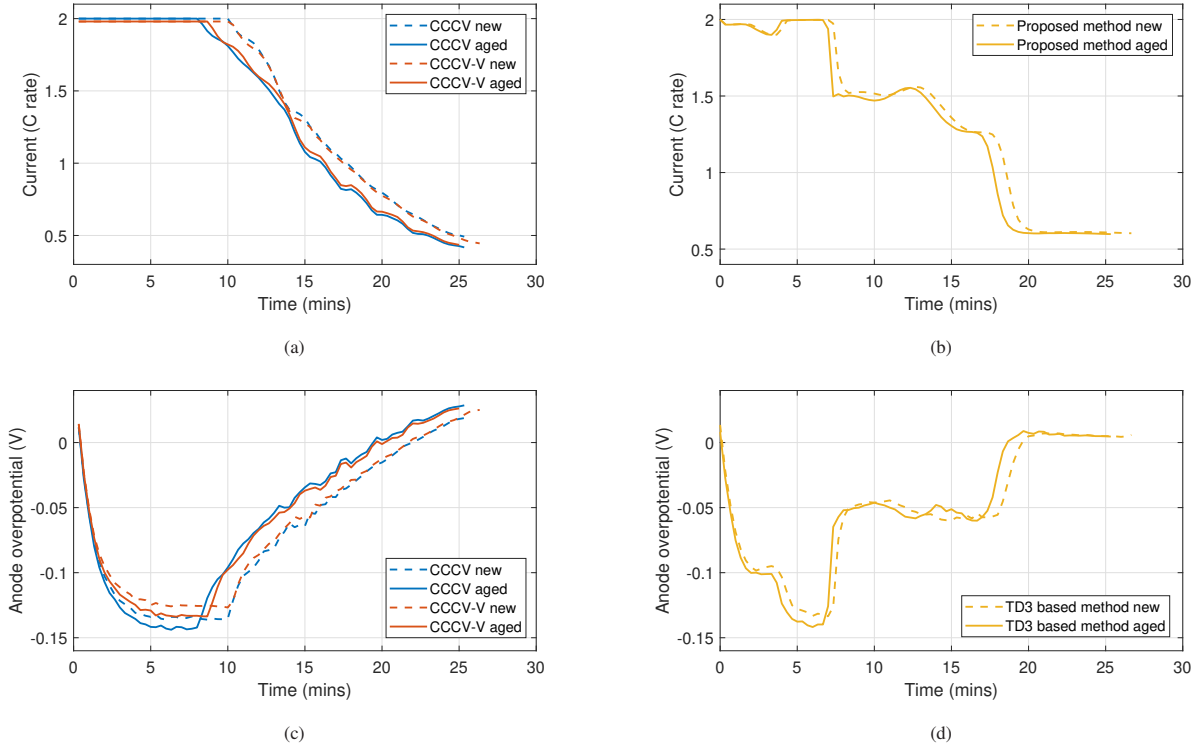


Figure 8: Current and anode potential profiles of the studied cell at different aging levels under different control methods.

5. Conclusion

In this paper, we present a novel health-aware fast charging strategy for lithium-ion batteries, based on a deep learning approach. Unlike conventional charging methods that primarily focus on minimizing charging time, our proposed approach explicitly considers the trade-off between fast charging and extending battery life. By leveraging a mapping between the charge end voltage and the SoH of the battery from a constant current and constant overpotential control, the proposed method incorporates SoH-dependent voltage into the optimal control decision-making process, effectively mitigating adverse degradation phenomena. To demonstrate the effectiveness of the proposed method, we utilized a high-fidelity single particle model with electrolyte implemented in PyBaMM. This model served as the test environment, capturing realistic degradation behaviors and allowing for robust evaluation across a full life-cycle

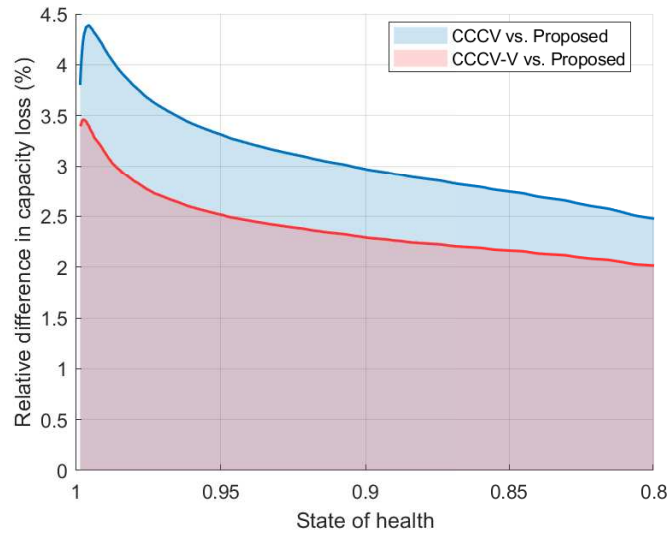


Figure 9: Relative difference in capacity loss due to lithium plating by comparing CC-CV and CC-CV-V to the proposed method. The positive value in y-axis means the least plated lithium triggered by the proposed method.

simulation. Comparisons with benchmark controllers demonstrate that the TD3-based policy successfully reduces overall degradation without significantly compromising charge speed, in a practical and implementable way.

Acknowledgement

This work was supported by Marie Skłodowska-Curie Actions Postdoctoral Fellowships under the Horizon Europe programme (Grant No. 101110832) and the Swedish Research Council (Grant No. 2023-04314). The authors would like to thank Dr Yang Li from the Chalmers University of Technology for his assistance with potential model simulation and setup in Matlab.

References

- [1] L. Zhang, C. Sun, G. Cai, L. H. Koh, Charging and discharging optimization strategy for electric vehicles considering elasticity demand response, *ETransportation* 18 (2023) 100262.
- [2] M. Armand, J.-M. Tarascon, Building better batteries, *Nature* 451 (7179) (2008) 652–657.
- [3] J. B. Goodenough, K.-S. Park, The Li-ion rechargeable battery: A perspective, *J. Am. Chem. Soc.* 135 (4) (2013) 1167–1176.
- [4] A. Ahmad, J. Meyboom, P. Bauer, Z. Qin, Techno-economic analysis of energy storage systems integrated with ultra-fast charging stations: A dutch case study, *eTransportation* (2025) 100411.
- [5] G. E. Blomgren, The development and future of lithium ion batteries, *J. Electrochem. Soc.* 164 (1) (2016) A5019.
- [6] H. Rahimi-Eichi, U. Ojha, F. Baronti, M.-Y. Chow, Battery management system: An overview of its application in the smart grid and electric vehicles, *IEEE Ind. Electron. Mag.* 7 (2) (2013) 4–16.
- [7] M. Broussely, P. Biensan, F. Bonhomme, P. Blanchard, S. Herreyre, K. Nechev, R. Staniewicz, Main aging mechanisms in Li ion batteries, *J. Power Sources* 146 (1-2) (2005) 90–96.

- [8] P. M. Attia, A. Grover, N. Jin, K. A. Severson, T. M. Markov, Y.-H. Liao, M. H. Chen, B. Cheong, N. Perkins, Z. Yang, et al., Closed-loop optimization of fast-charging protocols for batteries with machine learning, *Nature* 578 (7795) (2020) 397–402.
- [9] G. L. Plett, *Battery management systems, Volume I: Battery modeling*, Artech House, 2015.
- [10] Y. Li, T. Wik, Y. Huang, C. Zou, Nonlinear model inversion-based output tracking control for battery fast charging, *IEEE Trans. Control Syst. Technol.* 32 (1) (2023) 225–240.
- [11] M. Yuan, A. Burman, C. Zou, Robust model predictive control of fast lithium-ion battery pretreatment for safe recycling, *arXiv preprint arXiv:2503.11857* (2025).
- [12] M. Doyle, T. F. Fuller, J. Newman, Modeling of galvanostatic charge and discharge of the lithium/polymer/insertion cell, *J. Electrochem. Soc.* 140 (6) (1993) 1526.
- [13] Z. Khalik, M. Donkers, J. Sturm, H. J. Bergveld, Parameter estimation of the doyle–fuller–newman model for lithium-ion batteries by parameter normalization, grouping, and sensitivity analysis, *J. Power Sources* 499 (2021) 229901.
- [14] P. W. Northrop, B. Suthar, V. Ramadesigan, S. Santhanagopalan, R. D. Braatz, V. R. Subramanian, Efficient simulation and reformulation of lithium-ion battery models for enabling electric transportation, *J. Electrochem. Soc.* 161 (8) (2014) E3149.
- [15] G. Hwang, N. Sitapure, J. Moon, H. Lee, S. Hwang, J. S.-I. Kwon, Model predictive control of lithium-ion batteries: Development of optimal charging profile for reduced intracycle capacity fade using an enhanced single particle model (SPM) with first-principled chemical/mechanical degradation mechanisms, *Chem. Eng. J.* 435 (2022) 134768.
- [16] S. J. Moura, F. B. Argomedeo, R. Klein, A. Mirtabatabaei, M. Krstic, Battery state estimation for a single particle model with electrolyte dynamics, *IEEE Trans. Control Syst. Technol.* 25 (2) (2016) 453–468.
- [17] S. G. Marquis, V. Sulzer, R. Timms, C. P. Please, S. J. Chapman, An asymptotic derivation of a single particle model with electrolyte, *J. Electrochem. Soc.* 166 (15) (2019) A3693.
- [18] J. Li, R. G. Landers, J. Park, A comprehensive single-particle-degradation model for battery state-of-health prediction, *J. Power Sources* 456 (2020) 227950.
- [19] W. Huang, Y. Ye, H. Chen, R. A. Vilá, A. Xiang, H. Wang, F. Liu, Z. Yu, J. Xu, Z. Zhang, et al., Onboard early detection and mitigation of lithium plating in fast-charging batteries, *Nat. Commun.* 13 (1) (2022) 7091.
- [20] N. Wassiliadis, J. Kriegler, K. A. Gamra, M. Lienkamp, Model-based health-aware fast charging to mitigate the risk of lithium plating and prolong the cycle life of lithium-ion batteries in electric vehicles, *J. Power Sources* 561 (2023) 232586.
- [21] X. Yang, Z. Wei, L. Du, Constant overpotential fast charging for lithium-ion battery with twin delayed DDPG algorithm, in: *2022 IEEE Transportation Electrification Conference & Expo (ITEC), 2022*, pp. 623–628.
- [22] Y. Lu, X. Han, Y. Li, X. Li, M. Ouyang, Health-aware fast charging for lithium-ion batteries: Model predictive control, lithium plating detection, and lifelong parameter updates, *IEEE Trans. Ind. Appl.* (2024).
- [23] Y. Zhang, T. Wik, J. Bergström, C. Zou, Machine learning-based lifelong estimation of lithium plating potential: A path to health-aware fastest battery charging, *Energy Storage Mater.* 74 (2025) 103877.
- [24] S. Park, A. Pozzi, M. Whitmeyer, H. Perez, A. Kandel, G. Kim, Y. Choi, W. T. Joe, D. M. Raimondo, S. Moura, A deep reinforcement learning framework for fast charging of Li-ion batteries, *IEEE Trans. Transp. Electr.* 8 (2) (2022) 2770–2784.
- [25] Z. Wei, Z. Quan, J. Wu, Y. Li, J. Pou, H. Zhong, Deep deterministic policy gradient-DRL enabled multiphysics-constrained fast charging of lithium-ion battery, *IEEE Trans. Ind. Electron.* 69 (3) (2021) 2588–2598.
- [26] Y. Hao, Q. Lu, X. Wang, B. Jiang, Adaptive model-based reinforcement learning for fast charging optimization of lithium-ion batteries, *IEEE Trans. Ind. Inform.* (2023).
- [27] V. Sulzer, S. G. Marquis, R. Timms, M. Robinson, S. J. Chapman, Python battery mathematical modelling (PyBaMM), *J. Open Res. Softw.* 9 (1) (2021).
- [28] L. Xia, E. Najafi, Z. Li, H. Bergveld, M. Donkers, A computationally efficient implementation of a full and reduced-order electrochemistry-based model for Li-ion batteries, *Appl. Energy* 208 (2017) 1285–1296.
- [29] Z. Khalik, M. Donkers, H. J. Bergveld, Model simplifications and their impact on computational complexity for an electrochemistry-based

- battery modeling toolbox, *J. Power Sources* 488 (2021) 229427.
- [30] H. Wang, Y. Song, X. Sun, S. Mo, C. Chen, J. Wang, Onboard in-situ warning and detection of Li plating for fast-charging batteries with deep learning, *Energy Storage Mater.* 71 (2024) 103585.
- [31] S. E. O’Kane, W. Ai, G. Madabattula, D. Alonso-Alvarez, R. Timms, V. Sulzer, J. S. Edge, B. Wu, G. J. Offer, M. Marinescu, Lithium-ion battery degradation: how to model it, *Phys. Chem. Chem. Phys.* 24 (13) (2022) 7909–7922.
- [32] P. Arora, M. Doyle, R. E. White, Mathematical modeling of the lithium deposition overcharge reaction in lithium-ion batteries using carbon-based negative electrodes, *J. Electrochem. Soc.* 146 (10) (1999) 3543.
- [33] C. von Lüdgers, J. Keil, M. Webersberger, A. Jossen, Modeling of lithium plating and lithium stripping in lithium-ion batteries, *J. Power Sources* 414 (2019) 41–47.
- [34] N. A. Chaturvedi, R. Klein, J. Christensen, J. Ahmed, A. Kojic, Algorithms for advanced battery-management systems, *IEEE Control Syst. Mag.* 30 (3) (2010) 49–68.
- [35] A. Tomaszewska, Z. Chu, X. Feng, S. O’kane, X. Liu, J. Chen, C. Ji, E. Endler, R. Li, L. Liu, et al., Lithium-ion battery fast charging: A review, *eTransportation* 1 (2019) 100011.
- [36] Y. Li, D. Karunathilake, D. M. Vilathgamuwa, Y. Mishra, T. W. Farrell, S. S. Choi, C. Zou, Model order reduction techniques for physics-based lithium-ion battery management: A survey, *IEEE Ind. Electron. Mag.* 16 (3) (2021) 36–51.
- [37] Y. Huang, C. Zou, Y. Li, T. Wik, MINN: Learning the dynamics of differential-algebraic equations and application to battery modeling, *IEEE Trans. Pattern Anal. Mach. Intell.* (2024).